IEEE Journal of Microwaves

Received 12 September 2020; revised 22 October 2020; accepted 26 October 2020.
Date of current version 7 January 2021.

Digital Object Identifier 10.1109/JMW.2020.3034583

Microwave Photonic Array Radars

SHILONG PAN (Senior Member, IEEE), XINGWEI YE (Student Member, IEEE), YAMEI ZHANG (Member, IEEE), AND FANGZHENG ZHANG (Senior Member, IEEE)

(Invited Paper)

Key Laboratory of Radar Imaging and Microwave Photonics, Ministry of Education, Nanjing University of Aeronautics and Astronautics, Nanjing 210016, China

CORRESPONDING AUTHOR: FANGZHENG ZHANG (e-mail: zhangfangzheng@nuaa.edu.cn).

This work was supported in part by the National Key R&D Program of China under Grant 2018YFB2201803, in part by the National Natural Science Foundation of China under Grant 61871214, and also in part by the Natural Science Foundation of Jiangsu Province under Grant BK20180066.

ABSTRACT Phased array radars have remarkable advantages over radars with single-element antenna in terms of agility, flexibility, robustness, and reconfigurability. Current pure-electronic phased array radars face challenges when operating with a large frequency tunable range and/or with broad instantaneous bandwidth. Microwave photonics, which allows wide bandwidth, flat frequency response, low transmission loss, and immunity to electromagnetic interference, is a promising solution to cope with issues faced by pure electronics. In this paper, we introduce a general architecture of microwave photonic array radar systems and review the recent advancement of optical beamforming networks. The key elements for modelling the response of the true time delay (TTD) and/or phase-shifting unit are presented and discussed. Two typical array antenna structures are introduced, i.e., microwave photonic phase shifter based array and optical true time delay based array, of which the principle and typical implementations are described. High-resolution inverse synthetic aperture radar (ISAR) imaging is also realized based on a microwave photonic array radar. The possibility of on-chip integration of the microwave photonic array radar is discussed.

INDEX TERMS Microwave photonics, radar, phased array, true time delay, beamforming, radar imaging.

I. INTRODUCTION

Phased array radars can be dated back to the 1930s [1]. A typical phased array is an array of antenna elements, of which the phase of the transmitted or received signal to/from each antenna element is controlled independently by a phase shifter [2]. The use of phased array technique is a great breakthrough for radar systems [3]–[6]. Compared with radars with single-element antenna, the radiation power and the equivalent aperture size of phased array radars are significantly improved, which boosts the detection distance and increases the angular resolution. The beam produced by the phased array radar can be scanned electronically, which brings distinct advantages over single-element mechanical scanning antenna in speed, flexibility, and reconfigurability. Despite the rapid development, phased array radar faces challenges when the radar carrier covers a broad frequency range, or the radar waveform has a large instantaneous bandwidth.

One of the most critical components in the phased array radar is a beamforming network. Fig. 1 illustrates the schematic diagram of the basic beamforming network for phased array radars, which is composed of N antennas incorporated with N phase shifters [7]. Adjacent antennas are separated by a distance of d. When the beam is steered to an angle of θ, we have

$$\Delta R = d \cdot \sin\theta \tag{1}$$

where ΔR is the minimum distance from the wavefront to the antenna elements. To let the signals radiated from the

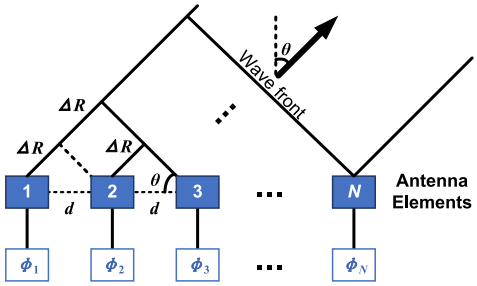

FIGURE 1. Basic beamforming network for phased array radars.

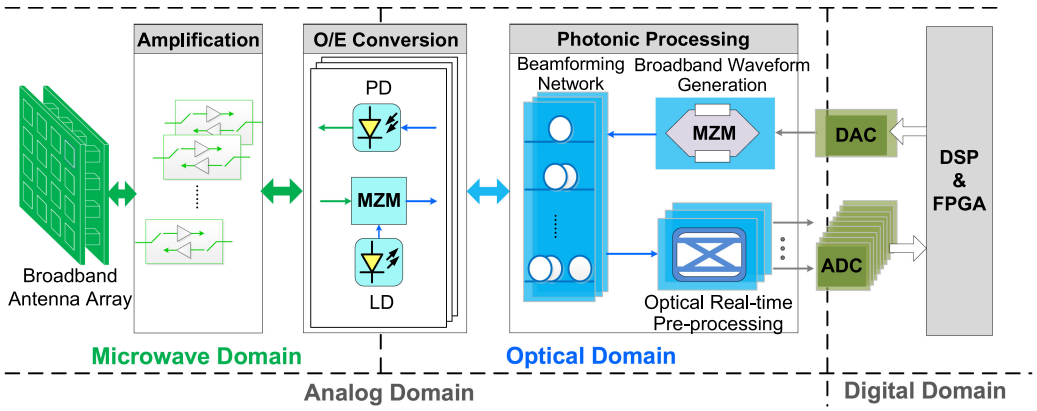

FIGURE 2. The architecture of a generic microwave photonic arrayed radar. LD: laser diode; PD: photodetector; MZM: Mach-Zehnder modulator; DAC: digital-to-analog converter; ADC: analog-to-digital convertor; DSP: digital signal processor; FPGA: field programmable gate array.

antennas have the same phase shifts at the wavefront, the phase difference between the adjacent antennas should satisfy

$$\Delta\phi = \frac{2\pi f \cdot \Delta R}{c} \tag{2}$$

where f is the frequency of the radiated signal. Substituting (2) to (1), we obtain

$$\theta = \arcsin\left(\frac{c \cdot \Delta\phi}{2\pi f d}\right) \tag{3}$$

As can be seen, the beam pointing angle θ is a function of the phase difference $\Delta\phi$, and thus it can be adjusted by the phase shifters.

However, (3) is feasible only for single-frequency or narrow-band signals, since the pointing angle is dependent on the frequency f. For multi-band radar or frequency-agile radar, even if it is operated in the mode of narrow instantaneous bandwidth, the carrier frequency covers a wide frequency range. The required devices such as broadband electrically controlled phase shifters would be expensive and usually have poor performance due to the non-uniform response over a large spectral range.

On the other hand, for radars that transmit broadband waveforms, which is essential to achieve a high range resolution, the frequency-dependent operation in (3) would result in beam squint problem, i.e., the beam directions for different frequencies are different [12]. This problem can be solved using true-time-delay-based beamforming networks [13]. Considering the relationship between the time delay and phase shift, the beam direction in (3) can be rewritten as

$$\theta = \arcsin\left(\Delta\tau \cdot \frac{c}{d}\right) \tag{4}$$

where $\Delta\tau$ is the time delay difference between adjacent antenna elements. Therefore, by controlling the time delays, frequency-independent broadband beamforming can be realized. Nevertheless, constructing a true time delay beamforming network using microwave delay lines is very difficult, mainly because of the considerable transmission loss and uneven frequency response. Microwave photonic technology, which uses photonic devices to generate, transmit, and process microwave signals [5], [10], provides a promising solution to the above problems. Fig. 2 shows the generic architecture for microwave photonic arrayed radars, which consists of broadband antenna arrays, microwave amplification chains, optoelectronic conversion modules, photonic processing units for signal generation, processing and beamforming, digital-to-analog or analog-to-digital converters, and digital signal processing modules. Compared with pure electronic technologies, current microwave photonic systems may have comparative or even worse performance in dynamic range and noise figure, but the advantages of microwave photonics for array radar are still attractive, which are mainly reflected in the following four aspects [11]–[16].

First, benefiting from the high-frequency and broadband operation capability of the optoelectronic devices and subsystems, microwave photonic array radar can have a large bandwidth of ~50 GHz. In addition, a very flat amplitude and phase response in such a frequency range can be achieved. This is attributed to the fact that a signal with tens of GHz bandwidth in the microwave band can be regarded as a relatively narrow-band signal when it is up-converted to an optical frequency around 200 THz. In this way, the problem of broadband impedance matching and broadband equalization in the microwave frequency band is relieved.

Second, the optical delay line, typically implemented by optical fiber, has very low transmission loss, which is particularly favorable for constructing a broadband true-time delay beamforming network. The transmission loss of a microwave coaxial cable is ~2 dB/m, while the typical loss for optical fiber is 0.0002 dB/m, four orders of magnitude lower. Even if the loss of electrical-to-optical and optical-to-electrical conversions is taken into consideration, microwave photonic systems still show much lower entire loss when applied in a large array.

Third, photonics provides more degrees of freedom for performing multiplexing, which opens the possibility for large-scale array radars with reduced hardware resources. In the optical domain, wavelength-division multiplexing, polarization

multiplexing, and spatial division multiplexing can be applied, in addition to the time-division multiplexing, frequency-division multiplexing, and code-division multiplexing in traditional electronic arrays.

Finally, the electromagnetic interference immunity property of the microwave photonic technology is helpful to improve the integration density of the array radar. In electronic phased arrays, electromagnetic shielding devices are required to reduce electromagnetic interference, which leads to a waste of space and extra cost. The microwave photonic devices, especially the optical delay line, are made of nonmetallic materials such as glass and plastics which are hardly affected by electromagnetic radiation below terahertz. Thus, electromagnetic shielding requirements of the broadband arrays can be effectively alleviated by introducing microwave photonic technologies.

In this paper, we introduce some of the recent progress of microwave photonic arrays intended for radar applications, which consists of a theoretical model capable of revealing the characteristics of the array in the broadband scenario and several approaches to implementing the microwave photonic arrays. These approaches can be classified into two categories. In the first category, the arrayed radar has a narrow instantaneous bandwidth while its carrier frequency is tunable in a large frequency range. Broadband microwave photonic phase shifters are required in this kind of phased array. The second category of microwave photonic arrays uses an optically controlled true time delay beamforming network to deal with the beam-squint problem for broadband radars. The advancement of photonic integrated techniques for array radars is also overviewed.

II. THEORETICAL MODEL FOR BROADBAND MICROWAVE PHOTONIC ARRAYS

The key components in a microwave photonic arrayed radar are the photonic processing unit connected to the antenna elements, as shown in Fig. 2. Phase shifters are typical examples of such units. For most arrays, each processing unit can be modeled as a linear time-invariant system, namely a filter with a frequency response of $H_\theta(\omega, n)$, in which θ represents the desired main lobe direction of the array, ω is the angular frequency, and n is the index number of the corresponding antenna. In phase-shifter-based arrays, the phase shift introduced by each processing unit is independent of the signal frequency, which means the ideal $H_\theta(\omega, n)$ of a phase-shifter-based array should take the form of a constant phase shift, given as

$$H_\theta(\omega, n)_{\mathrm{PS}} = \exp\left[j\frac{1}{c}n\omega_0 d\sin\theta\right] \tag{5}$$

where ω_0 denotes the center angular frequency of the signal. For true-time-delay-based arrays, frequency-dependent phase shifts should be implemented, and the ideal $H_\theta(\omega, n)$ can be expressed as

$$H_\theta(\omega, n)_{\mathrm{TTD}} = \exp\left[j\frac{1}{c}n\omega d\sin\theta\right] \tag{6}$$

Different from the constant value in (5), the phase shift in (6) changes linearly with the angular frequency, which signifies the true-time-delay feature and thus broadens the bandwidth of the array.

In order to evaluate the performance of the entire array, the responses of the processing units are superposed with different time delays

$$H_{2\mathrm{D},\theta}(\omega, \varphi) = \sum_n H_\theta(\omega, n) \cdot \exp(j\tau_n\omega) \tag{7}$$

in which

$$\tau_n = \frac{1}{c}nd\sin\varphi \tag{8}$$

is the differential spatial delay between the nth antenna element and the array reference point when a fictitious receiver is placed on the angle of φ in the far-field zone. In (7), it is worthy to note that the characteristics of the array with the main lobe oriented to the angle of θ can be analyzed through a complex-valued response function that has two independent variables of the temporal angular frequency ω and the far-field observation angle φ. In fact, the two-dimensional response function $H_{2\mathrm{D},\theta}(\omega, \varphi)$ can be regarded as the generalization in the broadband scenario for the array factor in the classical narrow-band array theory, in which ω is adopted as a new independent variable to reveal the performance variation among a broad bandwidth.

Although the definition of the theoretical model in (7) is based on the assumptions of ideally identical antenna elements with isotropic radiation pattern, frequency-independent response, and accurate geometric arrangement, the model is still acceptable in the study of microwave photonic arrays since it can fully reflect the influence of each photonic processing unit on the array performance. Thus, we can use the model as the framework for simulation of microwave photonic array, separating the systematic simulation into the stage of unit simulation and the stage of beamforming simulation. In addition, the theoretical model is beneficial to the hardware-in-the-loop simulation of a microwave photonic array, in which frequency responses of the units, i.e., $H_\theta(\omega, n)$, are obtained through experiment, and array characteristics such as radiation patterns could be simply calculated instead of being measured in an anechoic chamber [17].

Here we provide some simulation results on the relationship between the array bandwidth and the scale of the subarray to demonstrate the usage of the theoretical model. Consider an array with 24 antenna elements, of which the center frequency and the distance between two adjacent elements are 20 GHz and 0.75 cm, respectively. The main lobe is oriented to 60°. Due to the periodic feature of phase control, it is much easier to implement beam steering by using phase shifters than using true time delay lines. However, as mentioned in Section I, the bandwidths of phase-shift-based arrays are severely limited. One of the solutions to this problem is to divide the array into several subarrays, in which phase shifters are employed within each subarray, and true time delay lines are adopted to

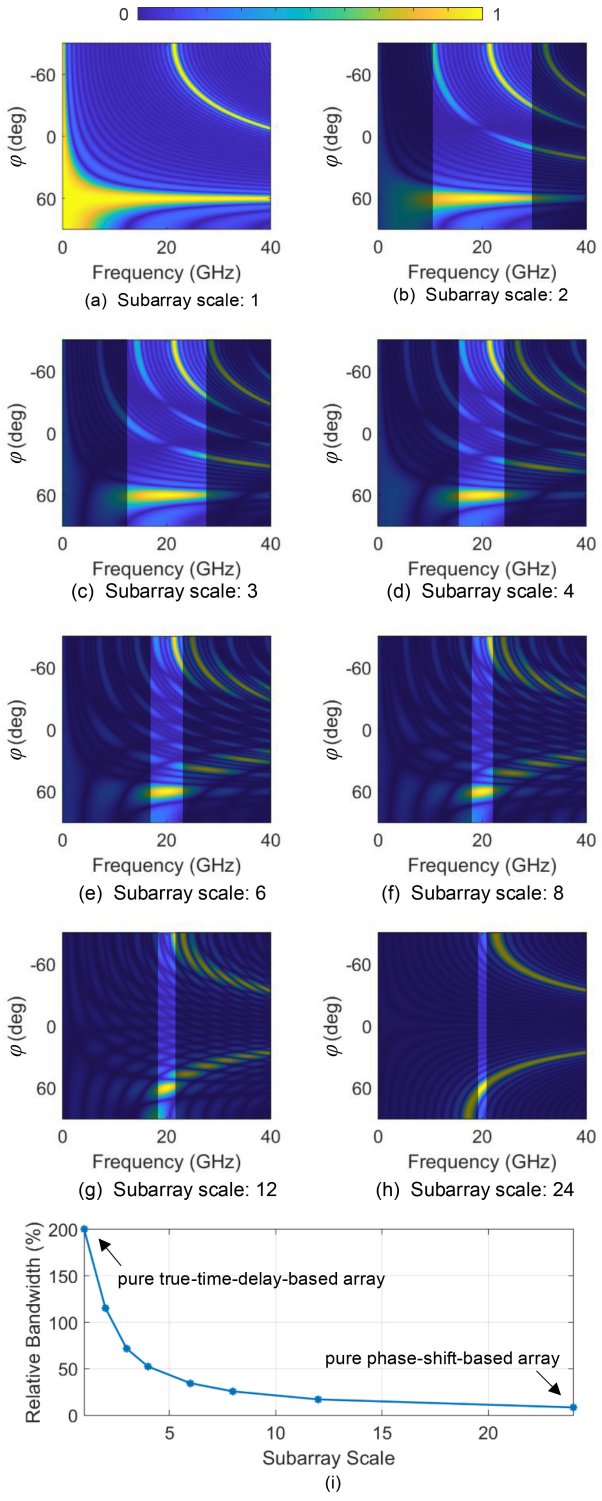

FIGURE 3. (a-h) Two-dimensional responses of a 24-element array with different subarrays, in which useful frequency bands are highlighted. (i) Relationship between the relative bandwidth of the array and the number of antenna elements in a subarray.

compensate for the differential time delays between the subarrays. Fig. 3(a)–3(h) depicts the simulated two-dimensional responses of the array with different subarray scales, in which the numbers of antenna elements in one subarray are 1 (pure true-time-delay-based array), 2, 3, 4, 6, 8, 12, and 24 (pure phase-shift-based array). Frequency bands around the center frequency of 20 GHz are highlighted to indicate the change in the useful bandwidths. From Fig. 3(a)–3(h), we can see that increasing phase-shift-based elements in a subarray leads to a decrease in the array bandwidth. The corresponding quantitative relationship is summarized in Fig. 3(i), in which the relative bandwidth is defined as the 3-dB array bandwidth divided by 20 GHz. It is obvious that if the scale of the subarray is larger than 4, the array can merely process signals with relative bandwidths below 50%.

Similarly, we can also use the theoretical model to study the impact of non-idealities in $H_\theta(\omega, n)$ on array performance. Some results addressing the optical dispersion-induced unwanted phase shift and the effects caused by realistic switches can be found in [18].

III. PHASED ARRAY BASED ON MICROWAVE PHOTONIC PHASE SHIFTERS

To meet the requirements of future multi-function or cognitive radar system, the phased array must have the capability to be operated in multiple frequency bands with good frequency agility. However, the performance of electronic devices constrains the spectral range of traditional phased arrays. Microwave photonic phase shifters can solve this problem by providing a very flat response over a large spectral range. In this section, different microwave photonic phase shifters are introduced, and a typical beamforming system based on microwave photonic phase shifters is presented.

A. MICROWAVE PHOTONIC PHASE SHIFTERS

In a microwave photonic phase shifter, the microwave signal is first converted into the optical domain, usually realized through electro-optical modulation. After signal processing with an optical device or a subsystem, optical-to-electrical conversion is implemented by a photodetector (PD) to get the microwave signal. The phase of the microwave signal is controlled by adjusting the parameters of the optical devices. In general, microwave photonic phase shifters can be divided into three categories, i.e., optical vector-sum technique, slow-light technique, and optical heterodyne technique.

The principle of the optical vector-sum phase shifter is to introduce an initial phase difference to two microwave signals and then combine them in the optical domain. By tuning the amplitude ratio between the two vector signals, the phase of the combined signal can be adjusted [19]–[22], as shown in Fig. 4. Reference [19] reported a typical optical vector-sum phase shifter, which is realized using two laser sources, a phase modulator (PM) and an optical bandpass filter (OBPF). By setting the wavelengths of the two lasers at the two slope edges of the OBPF, phase modulation to intensity modulation conversion is realized. Thanks to the nonlinear phase response of the OBPF, different phase shifts are introduced to the optical wavelengths and sidebands. After photodetection, two microwave signals with a phase difference can be obtained. By adjusting the power of the laser sources, the amplitudes

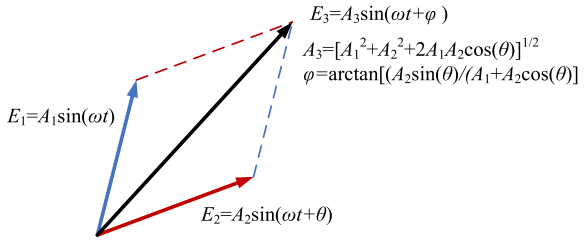

FIGURE 4. Principle of vector-sum based phase shifter.

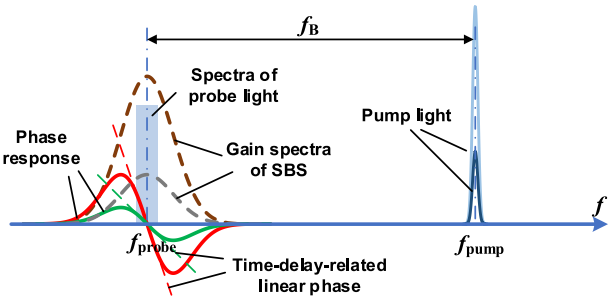

FIGURE 5. Principle of microwave photonic phase shifters based on SBS.

of the two microwave signals can be modified, leading to a tunable phase of the combined microwave signal at the output of the PD. The phase shifter has a large operation spectral range of over 30–60 GHz. The optical vector-sum method is very simple, but it suffers from severe power variation, and the configuration is usually complex and unstable.

The key to implementing slow-light-based microwave photonic phase shifters is to change the group delay index of the transmission medium [23]–[31]. One such system is realized based on the stimulated Brillouin scattering (SBS) effect in a highly nonlinear medium [23]–[27]. The principle is illustrated in Fig. 5. When a probe light with a wavelength of f_{probe} and a pump light at $f_{pump} = f_{probe} + f_B$, where f_B is the Brillouin frequency shift, are injected into the fiber, SBS effect would be stimulated, of which an optical gain is excited around f_{probe} accompanied with a violent phase variation. The phase is varied linearly versus the optical frequency around f_{probe}, producing a time delay that is related to the slope of the phase variation. By tuning the pump power to adjust the phase variation slope, the time delay, as well as the phase of the microwave signal, can be changed. Based on this principle, an SBS-based microwave phase shifter was built with a phase tuning range of 168 degree and an operating frequency range over 1–18 GHz [23].

In addition to SBS, semiconductor optical amplifiers (SOAs) [28]–[30], nonlinear optical loop mirrors [31], and micro-ring resonators (MRRs) [32]–[34] can also be used to implement slow-light based phase shifters. For example, in [28], a microwave photonic phase shifter using three SOAs and a fiber Bragg grating (FBG) is established, which achieved a maximum phase shift of 360 degree over a 40-GHz frequency range [29].

Optical heterodyne based microwave photonic phase shifter is usually realized by introducing a phase difference to two

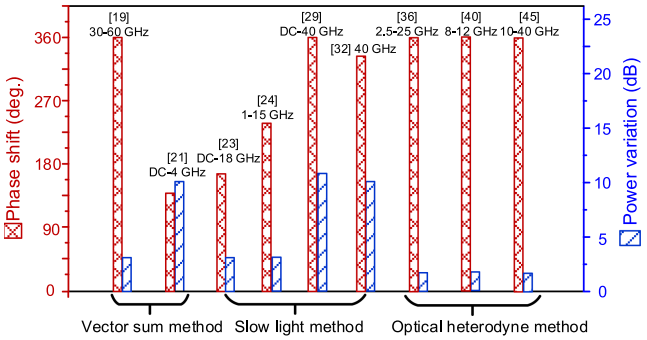

FIGURE 6. Performance comparison of the microwave photonic phase shifters realized by the three methods in [19], [21], [23], [24], [29], [32], [36], [40], and [45].

phase-correlated optical wavelengths [35]–[43]. After photodetection, the optical phase difference would be mapped to the phase of the generated microwave signal. In order to introduce a phase difference to the two optical wavelengths, an FBG is generally used to separate them into two branches, and an electro-optical PM is applied in one branch to adjust the phase [36]. However, the spatial separation of the two optical wavelengths would deteriorate the stability of the system. To remedy this, a Sagnac loop incorporated with a PM and an FBG was employed [37], [38], in which two optical carriers generated by the electrical-optical modulation are counter-propagated in the loop, experiencing the same environmental variation. Thanks to the uni-traveling characteristics of the PM, different phases are imposed on the two optical carriers. Besides, this kind of microwave photonic phase shifters can also be realized when the two optical wavelengths are separated in two sub-modulators [39], [40] of an integrated modulator or along with two orthogonal polarization directions of a polarization-sensitive modulator [35], [41]–[45]. By controlling the DC bias of the electro-optical modulator or the state-of-polarization of the signal, different phase shifts can be introduced to the two optical wavelengths. As a result, a microwave photonic phase shifter can be implemented.

Fig. 6 shows the performance comparison of the microwave photonic phase shifters realized by the aforementioned methods, in which the maximum phase shift, the operation bandwidth, and the power variation are considered. For all the three photonic phase-shifting methods, the maximum operation bandwidth is typically limited by the bandwidth of the electro-optical modulators (EOMs) and PDs, which can reach 50 GHz or more. Thus, the experimental demonstrations in Fig. 6 may not reflect the large bandwidth provided by photonic systems. In Fig. 6, it is also found that the optical heterodyne method can easily achieve full-360-degree phase-shifting while the phase-shifting range of the other two methods is smaller.

B. MICROWAVE PHOTONIC PHASE SHIFTER BASED BEAMFORMING NETWROK

Based on the broadband microwave photonic phase shifters, a radar beamforming network with a broad spectral range can be constructed. In this section, we show a typical beamforming

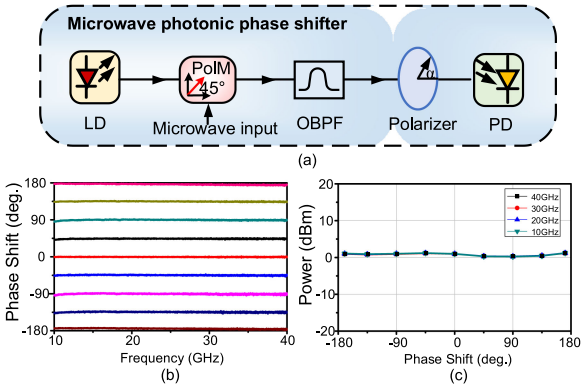

FIGURE 7. (a) Schematic diagram of the microwave photonic phase shifter based on polarization modulation; (b) Phase response of the phase shifter at different polarization settings; (c) Output power as a function of the phase shift at different frequencies (the four curves are superimposed).

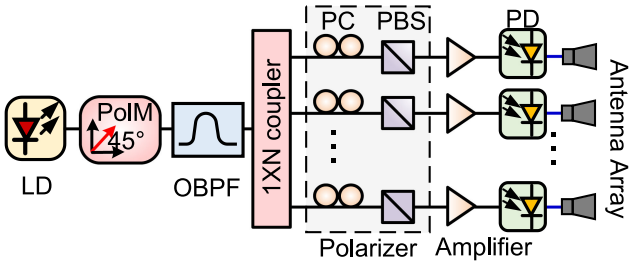

FIGURE 8. The schematic diagram of the phased array antenna based on the polarization-modulated microwave photonic phase shifter.

system constructed by a multi-channel microwave photonic phase shifter realized based on electro-optical polarization modulations [44], [45].

Fig. 7(a) shows the configuration of the microwave photonic phase shifter [45], which is consisted of a laser diode (LD), a polarization modulator (PolM), an OBPF, a polarizer, and a PD. The LD, PolM, and OBPF are used to realize optical single-sideband polarization modulation (OSSB-PolM) [46]. The OSSB-PolM signal is composed of two orthogonal-circularly polarized wavelengths that can be expressed as $\exp(j\omega_1 t)$ $(j\hat{x}+\hat{y})$ and $\exp(j\omega_2 t)$ $(-j\hat{x}+\hat{y})$, where ω_1 and ω_2 are the angular frequencies. After a polarizer with a polarization direction of α to x-axis, the two orthogonal-circularly polarized wavelengths would change to $\exp(j\omega_1 t+j\alpha)+\exp(j\omega_2 t-j\alpha)$. After photodetection, the phase difference 2α between the two wavelengths would be converted to the phase of the generated microwave signal. By adjusting the polarization angle α of the polarizer, the phase of the obtained microwave signal can be continuously tuned from 0 to 360 degree. In a proof-of-concept experiment, a full-range tunable phase shift in a frequency range of 10–43 GHz was achieved, and the power variation was kept within 1 dB, as shown in Figs. 7(b) and (c).

Based on the polarization-modulated microwave photonic phase shifter, a phased array is established [47], as shown in Fig. 8. Thanks to the excellent scalability of the polarization-modulated microwave photonic phase shifter, the OSSB-PolM

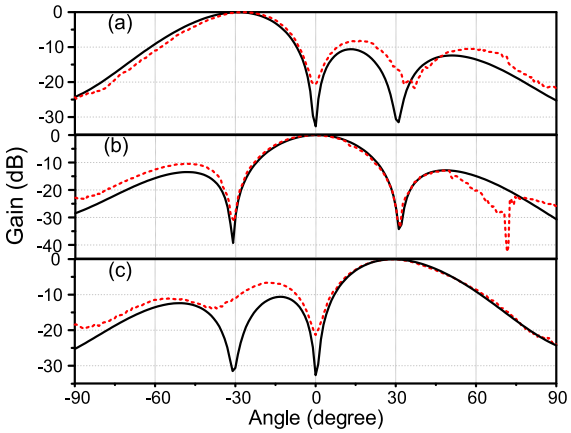

FIGURE 9. The simulated and experimentally measured radiation patterns of the phased array antenna when the angle of the beam is (a) −30°, (b) 0°, and (c) 30°. (The black-solid and the red-dotted curves are the simulated and experimental results, respectively)

signal is split into N branches to build an N-channel phase shifter. In each branch, a polarization controller (PC) and a polarization beam splitter (PBS) are used to serve as a polarizer, which is tuned to adjust the phase shift of each channel. An optical amplifier is connected in each channel to boost the optical power. The N microwave phase shifters share the same laser source and modulator, making the system compact and cost-effective. The obtained N phase-shifted microwave signals are emitted to the free space through an antenna array.

In the experimental demonstration, a 4-element linear patch antenna array and a 1×4 optical controlled beamforming network are employed to construct the phased array antenna. The antenna array has a center frequency of 14 GHz and a 10-dB bandwidth of 500 MHz. Four phase-shifted signals at the frequency of 14 GHz are generated by the 4-channel microwave photonic phase shifter, which are radiated to the free space via the antenna array on an antenna turntable. By carefully setting the phase shifts of each radiated signal via adjusting the four polarizers, different radiation patterns can be obtained. Fig. 9 shows the measured radiation patterns (red-dotted curves) when the phase shifts are set to be [0°, 84°, 168°, −106°], [0°, 0°, 0°, 0°], and [0°, −84°, −168°, 106°], which result in radiation angles of −30°, 0°, and 30°, respectively. The simulated radiation patterns are also displayed as the black-solid curves. As can be seen, all the main lobes of the measured radiation patterns agree well with the simulated radiation patterns, and the pointing directions are steered to the desired angles. The 3-dB widths of the main lobes are 30° (−45° to −15°), 26° (−13° to 13°), and 30° (15° to 45°), respectively.

IV. ARRAY RADAR BASED ON OPTICAL TRUE TIME DELAYS

True time delay technique is essential for broadband beamforming in an array radar. The photonics-based true time delay technique has distinct advantages over electrical delay lines thanks to the low transmission loss and the ultra-flat frequency

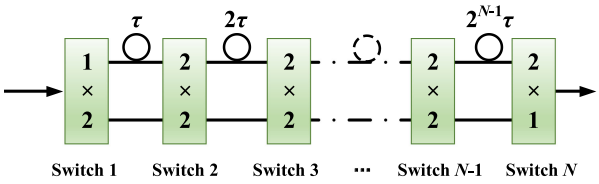

FIGURE 10. Optical switch based true time delay module.

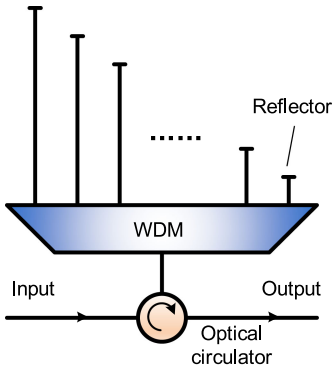

FIGURE 11. A typical wavelength-dependent true time delay module.

response of optical delay lines. In this section, the techniques for achieving optical true time delays are overviewed. A compact 2D optical beamforming network and a multi-band and multi-beam array antenna are introduced.

A. OPTICAL TRUE TIME DELAY MODULES

The basic function of optical true time delay modules is to control the time delay of optical signals carrying microwave information. Previously, three typical approaches for implementing the optical true time delay were reported, i.e., optical path switching, dispersive elements, and optical devices with adjustable phase response.

Switching the optical path with different lengths is an intuitive way to realize optical true time delay. The optical path can be a free-space path [48] or an optical fiber [49]. To achieve a large time delay with high resolution and reduced number of optical components, N optical switches can be cascaded to achieve 2^N time delays, as shown in Fig. 10. The optical switch can be realized in a variety of ways, including electro-optical switch, magneto-optical switch [50], thermo-optical switch [51], and micro-electromechanical system (MEMS) switch [52]. Generally, optical switches with a fast switching speed and a high extinction ratio are required. The optical path switching based time delay can also be implemented using tunable lasers together with wavelength-dependent true time delay devices [53], [54]. Fig. 11 shows a typical implementation [55], [56], in which different wavelengths pass through different fiber lengths with the help of an optical wavelength-division multiplexer (WDM). Various delays can be achieved by tuning the wavelength. In addition, cascaded FBGs can also be used for wavelength-dependent

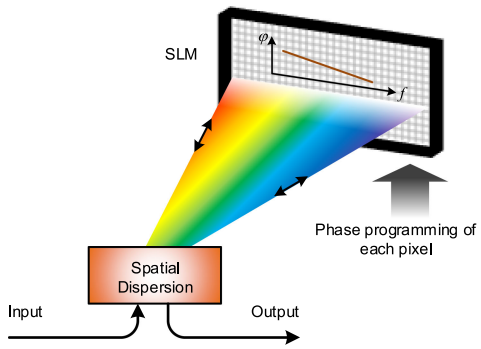

FIGURE 12. Optical true time delay based on a spatial light modulator (SLM).

true time delay, in which different wavelengths are reflected at different positions to introduce switchable delays [57].

The second method for obtaining optical true time delay is to apply an optical dispersive element, which introduces a wavelength-dependent true time delay. Different from the optical path switching method, which produces discrete time delays, the dispersion-based true time delay can be continuously tuned by changing the optical wavelength. Typical dispersive devices for true time delay include single-mode fibers, linearly-chirped FBGs [58], [59], photonic crystal fibers [60], and few-mode fibers [61]. Together with the wavelength division multiplexing technique, multiple microwave signals carried by different wavelengths can easily experience different time delays within the same dispersion media. A potential problem with this method is that a large dispersion would result in frequency-dependent microwave power fading [62]. To address this problem, an optical single-sideband (SSB) modulation technique can be applied [63], [64]. However, when using SSB modulation, the nonlinear phase-frequency response would lead to signal distortions, which can be compensated by connecting a series of multi-channel chirped FBGs with periodic time delay response to an ordinarily chirped FBG. This way, a stepped time delay response without phase distortions can be achieved [65].

The third method for achieving optical true time delay is to modify the phase response of an optical device. Because group delay is equal to the derivative of phase with respect to frequency, the true time delay can be realized if the slope of the phase response of an optical device is adjustable. Different from the dispersive-element-based approach, lasers with fixed wavelengths can be applied in this method. Fig. 12 shows a typical implementation based on a spatial light modulator (SLM). Different frequency components of the input optical signal are first projected to different pixels of the SLM through a spatial dispersive device, such as an acousto-optic modulator [66] or a dispersive grating [67]. A linear phase-frequency response is imposed on the optical signal by programming the phase of each pixel in the SLM. Then, all these optical frequency components are combined at the same dispersive device to get the time-delayed optical signal. Slow light effect is another way to achieve the adjustable phase response. The

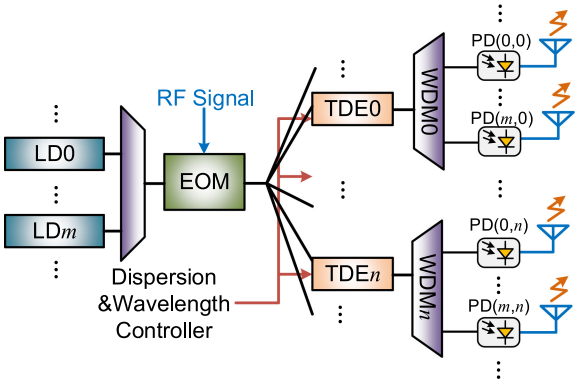

FIGURE 13. Schematic diagram of the compact photonic beamformer for 2D beam steering.

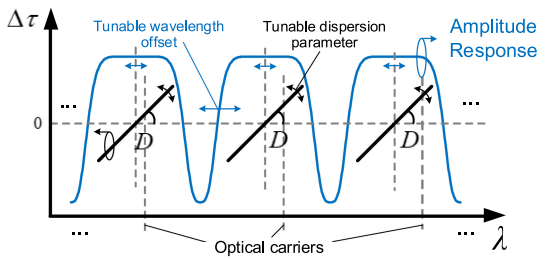

FIGURE 14. Typical responses of a TDE. TDE: tunable dispersive element.

principle of slow light effect has already been introduced in Section II. One critical problem of the slow light induced true time delay is its Lorentzian-shaped profile, which is only feasible for handling narrow-band microwave signals. To overcome this problem, solutions to extend the bandwidth were proposed. For example, by using a broadband optical pump signal in the SBS-based slow light system, a true time delay of 230 ps for a microwave signal with 1-GHz instantaneous bandwidth was achieved [68], [69].

B. BROADBAND 2D BEAMFORMING

The purpose of establishing an optical true time delay based broadband beamforming network is to simultaneously control the time delays of multiple RF signals that is fed to or captured by an antenna array. Here we introduce a dispersion-based optical true time delay beamforming structure, in which the time delays are adjusted through tuning optical dispersive elements.

For a planar array with antenna elements located along a rectangular grid on the xOy plane, a qualified beamformer is expected to implement tunable step-time delays along both the Ox and the Oy axes so that the main lobe of the array can be steered along both the elevation and the azimuth directions. To this end, we demonstrate a compact photonic RF beamformer with the schematic diagram shown in Fig. 13 [70]. When applied to an $M\times N$ array, the beamformer contains M lasers with different wavelengths and N tunable dispersive elements (TDEs), which are thermally-tuned chirped FBGs. The optical carriers generated by the lasers are combined and then modulated by an RF signal with an EOM. The obtained optical microwave signal is divided into N channels, and the signal in each channel is sent to a TDE for delay controlling. The output signals from each TDE are separated into multiple channels by a WDM demultiplexer according to their wavelengths. Finally, delayed RF signals serving as the feedings to the array are generated after optical-to-electrical conversion at multiple PDs.

The principle of the delay controlling in a TDE is illustrated in Fig. 14. The group delay response of the TDE is periodic and has multiple identical passbands. To implement step-time delays, the differential wavelength between two adjacent laser sources is set to be slightly different from the free spectral range (FSR) of the TDE, which could account for the increasing wavelength interval between the optical carriers and the corresponding channel centers, as shown in Fig. 14. Thus, step-time delays of signals with different optical carriers can be controlled by adjusting the dispersion parameter of one TDE. In addition, if the wavelength offsets of several TDEs in the beamformer are configured with step values, step-time delays can be achieved for signals with an identical optical carrier in different TDEs. Thanks to the thermal management, the dispersion parameter and the wavelength offset of the TDE can be adjusted independently, which means step-time delay control along with two directions and 2D beam steering can be realized without the need for a second-stage true time delay unit. It should be noted that the maximum bandwidth of this dispersion-based true-time delay is limited by the spectral width of each passband of the TDE.

A photonic beamformer for a 2 × 2 planar array is established. A pulsed RF signal is used as the driving signal of the modulator. Four delayed RF signals from four PDs are recorded by an oscilloscope and are used to calculate the radiation patterns of the array. Since the signal processed by the photonic beamformer is a broadband one, the performance of the beamformer can be evaluated through a correlation-maximum pattern (CMP) which is defined by the peak value of the cross-correlation of the beamformer input and the far-field signal on a specific direction [17], [18]. Fig. 15 shows the calculated 3D CMPs and the corresponding cross-sections with the target main lobe oriented to $(\theta, \phi) = (45°, 135°)$ and $(\theta, \phi) = (30°, -60°)$. The results from the measured signals and the signals with ideal time delays are depicted as blue-solid curves and red-dashed curves, respectively. As can be seen, the directions of the main lobes match well with the ideal ones, which verifies the feasibility of the proposed beamformer.

C. BROADBAND MULTI-BAND AND MULTI-BEAM STEERING

The aforementioned photonic 2D beamformer has a compact structure but cannot steer multiple RF beams simultaneously. We have also proposed another beamforming network that can perform multi-beam steering. The network is mainly composed of an array of optical true time delay units, and each

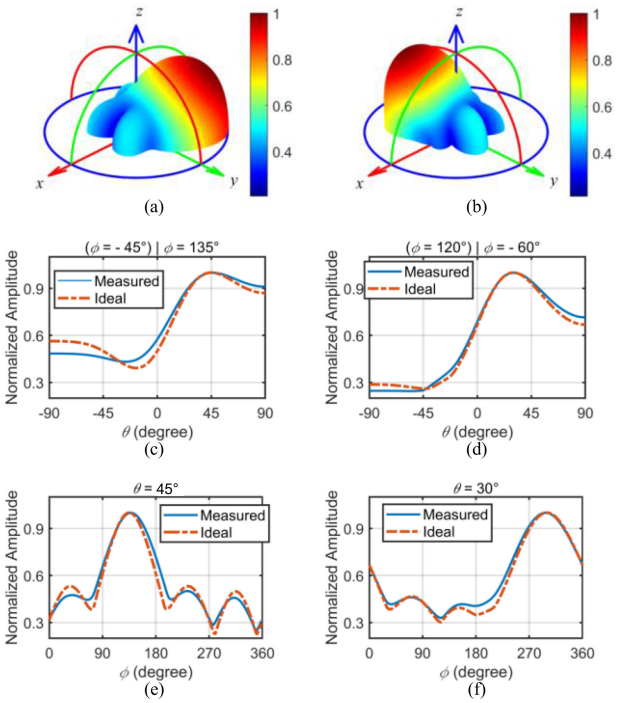

FIGURE 15. Correlation-maximum pattern of the photonic 2D beamformer with the main lobe steered to (a, c, e) $(\theta,\phi) = (45°, 135°)$ and (b, d, f) $(\theta,\phi) = (30°,-60°)$. (a, b) 3D patterns; (c, d) cross-sections along θ-direction; (e, f) cross-sections along ϕ-direction.

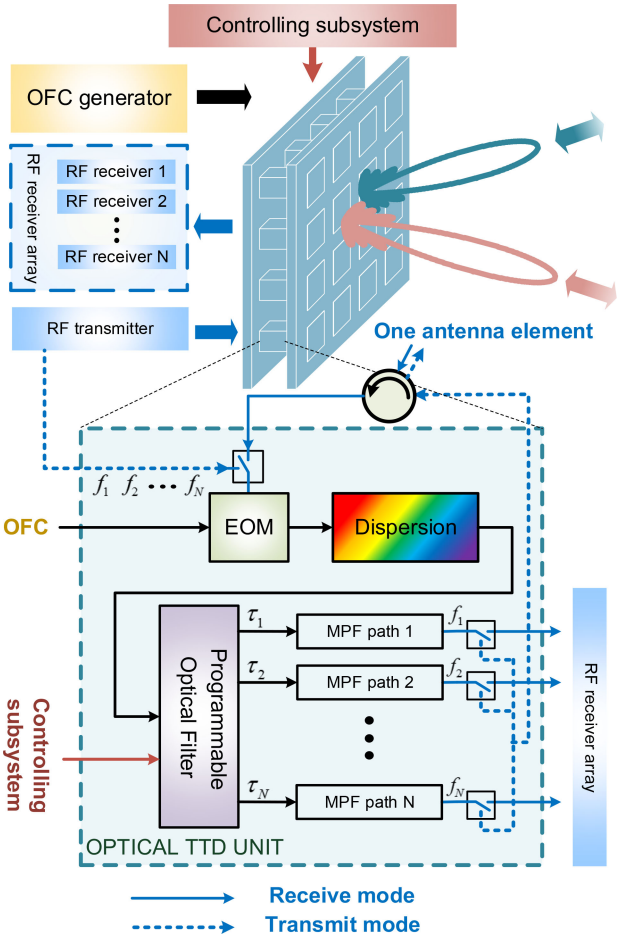

FIGURE 16. Concept of the multi-band and multi-beam steering network.

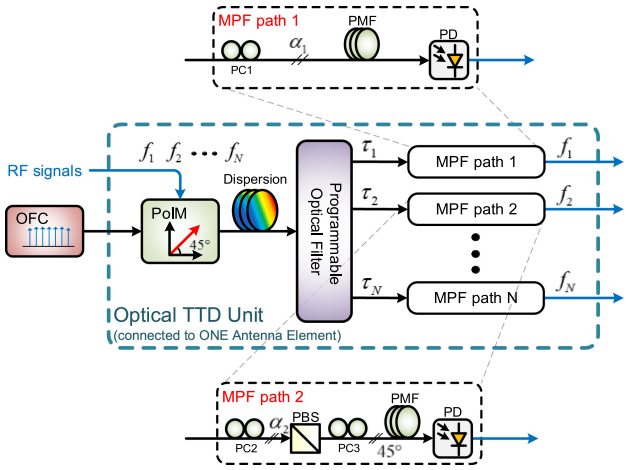

FIGURE 17. Detailed structure of the optical true time delay unit built in the experiment.

unit is capable of introducing different time delays to multiple RF signals concurrently [71]. Fig. 16 shows the structure of the proposed network. In the transmit mode, RF signals to be radiated are divided and sent to the optical true time delay units. All the units share the same optical source which is an optical frequency comb (OFC) consisting of plenty of frequency components (i.e., the comb lines). In each unit, the OFC is modulated by the RF signals through an EOM. Thanks to the large number of wavelengths provided by the OFC, RF signals with a variety of time delays can be achieved at the output port of the dispersive element. Afterward, two stages of filtering are implemented to assign different time delays to RF signals with specific frequencies. The first one is implemented in the optical domain using a programmable optical filter to determine the time delay, while the second one is achieved by microwave photonic filters (MPFs) with different passbands to rejecting unwanted RF frequency components. The obtained multiple RF signals are directed to the corresponding antenna element for radiation. Similarly, in the receive mode, RF signals from each antenna element are processed by its corresponding optical true time delay unit. The superposition of the signals from different units is carried out in the electrical domain.

In order to demonstrate the concept of the multi-beam steering network, an optical true time delay unit with two paths is built, of which the detailed structure is illustrated in Fig. 17. In the experimental unit, MPF1 has two taps with tap coefficients of $\{1, -1\}$ to realizing high-pass response [72]. The time delay between the two taps is brought by a spool of polarization maintaining fiber (PMF). In MPF2, a polarization beam splitter (PBS) is employed to select the signal along one polarization direction, which is then oriented to the two

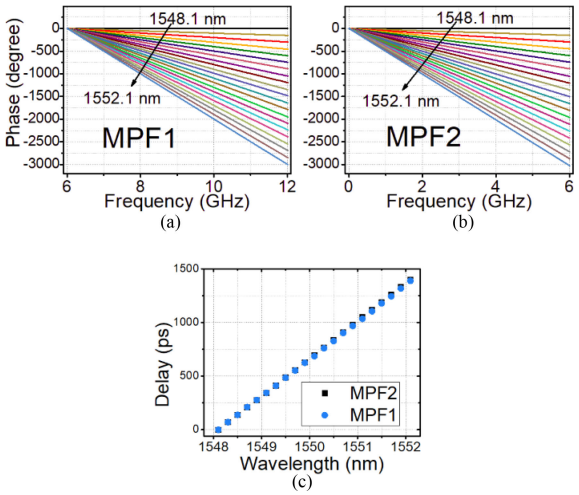

FIGURE 18. Phase responses of (a) MPF1 (high-pass) and (b) MPF2 (low-pass); (c) corresponded time delays.

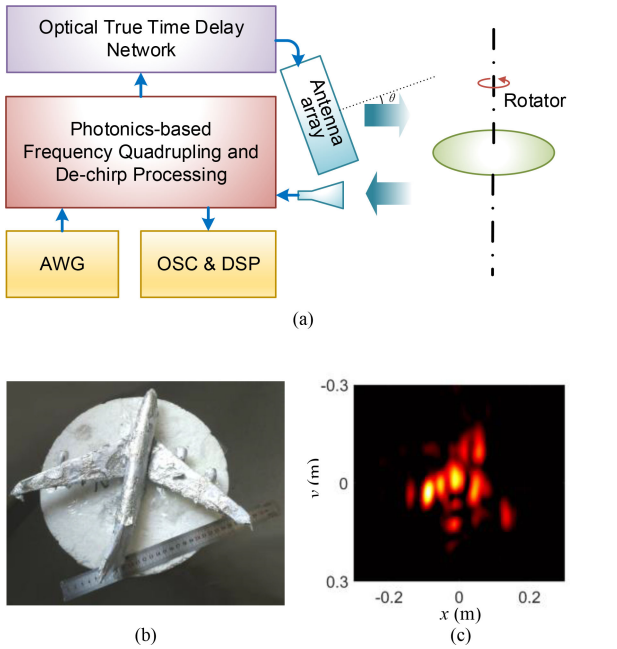

FIGURE 19. Schematic diagram of the microwave photonic array radar for target imaging; (b) Photograph of the target (a plane model); and (c) the imaging result. AWG: arbitrary waveform generator; OSC: oscilloscope.

polarization axes of a PMF by carefully aligning its state-of-polarization to have an angle of 45° to the principal axis of the PMF. Thus, a two-tap MPF (MPF2) with in-phase coefficients of {1, 1} is achieved to realize low-pass frequency response. It should be noted that the modulator used in the optical true time delay unit is a PolM, which means the responses of the MPFs can be improved by moving the dispersion fading nulls into unwanted frequency bands [73]. The performance of the optical true time delay unit is studied by measuring its complex-valued responses, i.e., magnitude responses and phase responses, under different comb line selections. The phase responses of the MPFs are depicted in Figs. 18(a) and (b), where they have a linear relationship with the RF frequency. This proves that the optical true time delay unit is broadband. The corresponding time delays can be calculated based on the phase responses, as shown in Fig. 18(c). The obtained time delay is proportional to the offset of the optical wavelength, which is consistent with the expectation, and the difference between the delay responses of MPF1 and MPF2 is negligible.

D. DEMONSTRATION OF MICROWAVE PHOTONIC ARRAY RADAR FOR IMAGING

In order to demonstrate the high-performance target detection of the microwave photonic array radar, we build up a prototype system with the structure shown in Fig. 19(a). High-resolution inverse synthetic aperture radar (ISAR) imaging is realized. A linear frequency modulated (LFM) signal generated from an arbitrary waveform generator is frequency-quadrupled through a photonic frequency-multiplication approach [74] and then sent to an optical true time delay network. In the network, the signal is divided into 16 paths with tunable time delays, of which the differential time delay between adjacent paths is determined by Eq. (4) in Section I. The obtained 16 signals with preset time delays are used for the feedings of a 16-element antenna array. Targets under radiation are placed on a rotator with a constant angular speed, which forms a simple geometric setup for ISAR imaging and could help to realize a higher azimuth resolution [75]. Echoes from targets are gathered by a single horn antenna. The analog processing of the echoes is also carried out in the optical domain, in which the photonics-based de-chirp operation is employed to remarkably compress the bandwidth of the signal. Such operation can also convert time delays of the echoes to peaks in the spectrum [74]. The de-chirped echoes are digitized by an oscilloscope, which enables ISAR algorithms conducted in the digital domain [75].

In the experiment, the LFM signal radiated by the antenna array has a bandwidth of 3 GHz at the K-band, which is achieved by frequency-quadrupling of a 750-MHz signal in the C-band. The target used for imaging is a plane model, of which the photograph is shown in Fig. 19(b). To verify the effectiveness of the optical true time delay network, the broadside direction of the array is set to deviate from the center of the rotator, and the delay parameters of the network are adjusted to steer the array main lobe to the target direction. The imaging result is provided in Fig. 19(c). As can be seen, the profile of the obtained ISAR image matches well with the target, which could validate the feasibility of the microwave photonic array radar.

V. INTEGRATED MICROWAVE PHOTONIC ARRAY

Photonic integration is necessary to make the microwave photonic arrays gain ground, which would lead to a similar or even better size, weight, and power consumption (SWaP) as compared with their electronic counterparts. Previously, many

works on integrated microwave photonics have been carried out to facilitate the practical application of the microwave photonic arrays. Thanks to the broadband beamforming capability, a lot of efforts have been devoted to construct integrated optical true time delay arrays. Only a few works are conducted for integrated arrays with microwave photonic phase shifters, which are interesting for radars with wide frequency tuning range but narrow instantaneous bandwidth. As an example, C. Porzi *et al.* demonstrated an integrated microwave photonic phase shifter based on the silicon on insulator (SOI) technology [76], which has a broad operational spectral range (>30 GHz), a large phase tuning range (up to 400 degree) and a fast switching speed (∼1 ns).

For integrated optical true time delay arrays, different materials have been used to fabricate the integrated delay element, such as silicon, lithium niobate, polymer, silicon nitride, silicon dioxide, and SOI. The basic principles are similar to those introduced in Section IV, which can be classified again into three categories.

In the first category, optical true time delays are achieved by integrated optical switches and waveguides with different lengths. For instance, a 4-bit reconfigurable true time delay chip was fabricated using four thermo-optical switches and a number of silicon nitride waveguides [77]. The chip has a size of 4.5 cm × 8.5 cm, but the time delay can reach 2.35 ns. Similarly, using thermo-optical switches and silicon delay lines, a 7-bit true time delay was achieved on a 7.4 mm × 1.8 mm chip, which could produce a maximum delay of 191.37 ps [78]. In addition to the thermo-optical switches, MEMS-based switches can also be integrated on a chip [79], [80]. The key problem associated with the thermo-optical and MEMS-based switches is their relatively slow switching speed, which is usually on the order of microsecond or millisecond. To achieve fast tuning speed, integrated optical true time delay based on electro-optical switches was also demonstrated [81], [82], in which the switching time was reduced to several nanoseconds.

The second kind of integrated optical true time delay is implemented by optical wavelength switching, typically in an array waveguide grating (AWG). In the AWG, different wavelengths pass through different channels with different optical lengths, enabling different true time delays. With this method, a 4-bit true time delay of up to 600 ps is achieved based on a perfluoropolymer optical integration platform [83]. In [84], by switching the optical wavelength over a 10-nm range in an SOI-based AWG, 2D beam scanning in the range of 15° × 50° was achieved. In another work, beam steering with a 186° scanning-angle range for a 38-GHz microwave signal was demonstrated using the integrated AWG [85].

Integrated ring resonators are promising elements for building optical true time delay chips [86]–[88]. By thermally tuning the coupling coefficient and the cavity length of the ring resonators [89], the slope of the linear phase response around the resonant frequency can be changed, producing a tunable true time delay. It should be noted that the bandwidth of the single ring resonator is usually small due to the Lorentzian-shaped profile. This problem can be solved by cascading

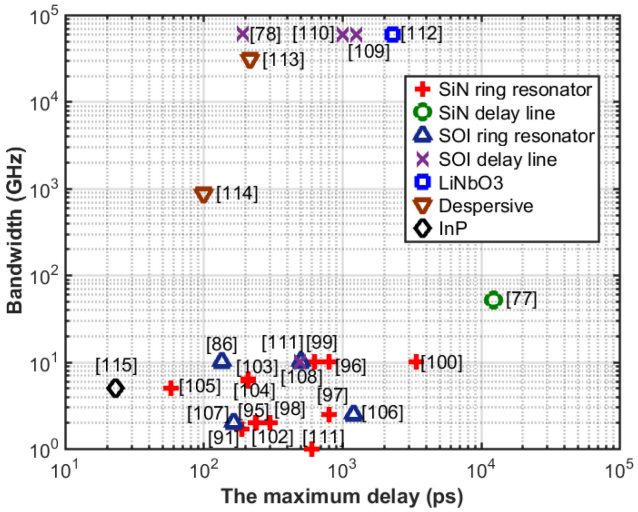

FIGURE 20. State-of-the-art of the integrated optical true time delays.

multiple ring resonators with different resonant frequencies. For example, twelve weakly coupled polymer ring resonators are cascaded in [90] to extend the operational bandwidth to 17 GHz. A tunable true time delay between 110 ps and 140 ps is achieved. In addition, by incorporating a reflector to the drop port of the MRR, a new type true time delay element with broadband group-delay response can be formed using a single resonator [91], [92]. The optical true time delay can also be realized by on-chip SBS-based slow-light [93], [94], by which a delay of 4 ns was achieved.

Fig. 20 shows the state-of-the-art of the integrated optical true time delays. It should be noted that the bandwidth of the optical true time delay line itself, no matter based on dispersive waveguide [113], [114] or waveguide with different length [78], [109]–[113], can be extremely high, since it is essentially frequency insensitive. When it is co-integrated with other electrooptic devices to realize a phased array radar, the upper limit of the operation bandwidth is finally determined by the electrooptic devices, e. g., the EOM or PD, which is typically lower than 40 GHz. As indicated by the results in Fig. 20, significant achievements have been achieved in recent years. However, the integrated optical true time delay is still facing a key problem of how to realize large time delay in a limited area. Moreover, for different techniques, the key issues to be solved are usually different. For example, for the methods realized by switching between multiple physical paths, the low-loss optical waveguide is essential. Although the transmission loss of some specialized Si_3N_4 (Si_3N_4/SiO_2), silicon (Silicon-pillars-supported structures), SOI (thick SOI), and $LiNbO_3$-on-insulator (using photolithography) waveguide reaches 0.45 dB/m [116], 0.08 ± 0.01 dB/m [117], 2.6 dB/m [118], and 3 dB/m [112], respectively, most of them are not compatible with the mature CMOS foundry, which leads to low yield, high fabrication cost and limited availability.

For true time delay realized by integrated ring resonators, strong resonance is necessary to achieve a large time delay, but this will inevitably limit the operation bandwidth [119]. Thus, breaking through the contradiction between a large time delay and a large operation bandwidth is necessary. Although the methods by cascading multiple resonators or using reflective resonators can enlarge the bandwidth, the time delay is still limited. A possible solution to this problem is to combine the optical switching-based true time delay technique with integrated ring resonators, so as to achieve a large and continuously adjustable true time delay. In this method, a large amount time delay with coarse adjustment is realized by optical switching-based technique, and fine delay adjustment is achieved by the integrated ring resonators. In this way, the requirement for both large time delay and large operation bandwidth can be greatly relaxed.

In fact, apart from the bandwidth and time delay amount, other issues should also be taken into consideration to realize an integrated microwave photonic array. For instance, the tuning speed of the optical true time delay module should be fast enough to ensure the high-speed scanning of the array radar. Thermal tuning is the easiest solution, but the tuning speed is quite limited. The electrical method can achieve high tuning speed, but it will introduce new restrictions to the material (e.g., requiring electro-optic nonlinear material) or the fabrication process (e.g., hybrid integration of PZT and SiN [119]). Furthermore, in addition to the optical true time delay module, other devices, such as laser, modulator, photodetector, should also be integrated to realize a fully-integrated microwave array, which is still a challenging problem from the current perspective.

VI. CONCLUSION

In conclusion, microwave photonic technologies for array radar systems were reviewed and discussed. The theoretical model, operational principle, and typical demonstrations based on discrete devices and photonic integration techniques were discussed for arrays working with a large frequency tunable range and/or with a large instantaneous bandwidth. Although there is still much work to do before widespread applications of the microwave photonic array radars, these technologies have successfully drawn attention from researchers from both the radar and photonic societies. We hope more efforts can be devoted to this field, particularly the photonic integration techniques, which may bring revolutionary promotion to future radars.

ACKNOWLEDGMENT

The authors would like to thank the following individuals from the Key Laboratory of Radar Imaging and Microwave Photonics, Nanjing University of Aeronautics and Astronautics: Bindong Gao for contribution to Section III; Yuewen Zhou and Jingzhan Shi for contribution to Section IV; and Zhenzhou Tang, Guanqun Sun, and Simin Li for contribution to Section V.

REFERENCES

[1] L. Stark, "Microwave theory of phased array antennas-A review," *Proc. IEEE*, vol. 62, no. 12, pp. 1661–1701, 1974.
[2] R. Mailloux, "Phased array theory and technology," *Proc. IEEE*, vol. 70, no. 3, pp. 246–291, 1982.
[3] C. Pell, "Phased-array radars," *IEE Rev.*, vol. 34, no. 9, pp. 363–367, 1988.
[4] R. Mailloux, "Synthesis lectures on antennas," in *Electronically Scanned Arrays*. San Rafael, CA, USA: Morgan & Claypool, vol. 2, 2007, pp. 1–82.
[5] S. Pan and Y. Zhang, "Microwave photonic radars," *J. Lightw. Technol.*, vol. 38, no. 19, pp. 5450–5484, Oct. 1, 2020, doi: 10.1109/JLT.2020.2993166.
[6] A. Oliner and G. Knittel, *Phased Array Antennas*, 2nd ed. Boston, MA, USA: Artech House, 1972.
[7] H. Visser, *Array and Phased Array Antenna Basics*. Hoboken, NJ, USA: Wiley, 2005.
[8] I. Frigyes and A. Seeds, "Optically generated true-time delay in phased-array antennas," *IEEE Trans. Microw. Theory Techn.*, vol. 43, no. 9, pp. 2378–2386, Sep. 1995.
[9] S. Shemi, T. Chu, and J. Rodarick, "Integrated true-time-delay-based ultra-wideband array processing," *IEEE Commun. Mag.*, vol. 46, no. 9, pp. 162–172, Sep. 2008.
[10] J. P. Yao, "Microwave photonics," *J. Lightw. Technol.*, vol. 27, no. 3, pp. 314–335, 2009.
[11] S. Yegnanarayanan, P. Trinh, and B. Jalali, "Recirculating photonic filter: A wavelength selective time-delay for phased-array antennas and wavelength code-division multiple access," *Opt. Lett.*, vol. 21, pp. 740–742, 1996.
[12] J. Capmany, J. Mora, I. Gasulla, J. Sancho, J. Lloret, and S. Sales, "Microwave photonic signal processing," *J. Lightw. Technol.*, vol. 31, no. 4, pp. 571–586, 2013.
[13] S. Pan, D. Zhu, and F. Zhang, "Microwave photonics for modern radar systems," *Trans. Nanjing Univ. Aeronaut. Astronaut.*, vol. 31, no. 3, pp. 219–240, 2014.
[14] S. Pan, D. Zhu, S. Liu, and K. Xu, "Satellite payloads pay off," *IEEE Microw. Mag.*, vol. 16, no. 8, pp. 61–73, Sep. 2015.
[15] D. Zhu, W. Chen, and S. L. Pan, "Photonics-enabled balanced hartley architecture for broadband image-reject microwave mixing," *Opt. Exp.*, vol. 26, no. 21, pp. 28022–28029, 2018.
[16] Z. Cao *et al.*, "Advanced integration techniques on broadband millimeter-wave beam steering for 5G wireless networks and beyond," *IEEE J. Quantum Electron.*, vol. 52, no. 1, Jan. 2016, Art. no. 0600620.
[17] X. Ye, B. Zhang, Y. Zhang, D. Zhu, and S. Pan, "Performance evaluation of optical beamforming-based wideband antenna array," *Chin. Opt. Lett.*, vol. 15, no. 1, Jan. 2017, Art. no. 010013.
[18] X. Ye, D. Zhu, Y. Zhang, S. Li, and S. Pan, "Analysis of photonics-based RF beamforming with large instantaneous bandwidth," *J. Lightw. Technol.*, vol. 35, no. 23, pp. 5010–5019, 2017.
[19] X. Wang, E. H. W. Chan, and R. Minasian, "All-optical photonic microwave phase shifter based on an optical filter with a nonlinear phase response," *J. Lightw. Technol.*, vol. 31, no. 20, pp. 3323–3330, 2013.
[20] W. Vogel and M. Berroth, "Liquid crystal phase shifter for optically generated RF-signals," in *Proc. 30th Eur. Microw. Conf.*, Paris, France, 2000, pp. 1–4.
[21] L. Bui, A. Mitchell, K. Ghorbani, and T. Chio, "Wideband RF photonic vector sum phase-shifter," *Electron. Lett.*, vol. 39, no. 6, pp. 536–537, 2003.
[22] X. Sun *et al.*, "Photonic RF phase shifter based on a vector-sum technique using stimulated brillouin scattering in dispersion shifted fiber," *IEEE Trans. Microw. Theory Techn.*, vol. 58, no. 11, pp. 3206–3212, Nov. 2010.
[23] A. Loayssa, S. Galech, and F. Lahoz, "Broadband microwave photonic phase-shifter based on stimulated Brillouin scattering," in *Proc. IEEE LEOS Annu. Meet. Conf.*, Sydney, NSW, Australia, 2005, pp. 839–840.
[24] M. Pagani, D. Marpaung, D. Y. Choi, S. J. Madden, B. Luther-Davies, and B. J. Eggleton, "Tunable wideband microwave photonic phase shifter using on-chip stimulated Brillouin scattering," *Opt. Exp.*, vol. 22, no. 23, pp. 28810–28818, 2014.
[25] M. Pagani, D. Marpaung, D. Choi, S. Madden, B. Luther-Davies, and B. Eggleton, "Tunable microwave photonic phase shifter using on-chip stimulated brillouin scattering," in *Proc. Conf. Lasers Electro Optics*, 2015, pp. 85–89.

[26] L. Thevenaz, "Slow and fast light in optical fibres," *Nature Photon.*, vol. 2, pp. 474–481, 2008.

[27] M. G. Herraez, K. Y. Song, and L. Thevenaz, "Arbitrary-bandwidth brillouin slow light in optical fibers," *Opt. Exp.*, vol. 14, no. 4, pp. 1395–1400, 2006.

[28] W. Xue, S. Sales, J. Capmany, and J. Mork, "Wideband 360° microwave photonic phase shifter based on slow light in semiconductor optical amplifiers," *Opt. Exp.*, vol. 18, no. 6, pp. 6156–6163, 2010.

[29] J. Sancho, J. Lloret, I. Gasulla, S. Sales, and J. Capmany, "Fully tunable 360 microwave photonic phase shifter based on a single semiconductor optical amplifier," *Opt. Exp.*, vol. 19, no. 18, pp. 17421–17426, 2011.

[30] P. Berger *et al.*, "Intermodulation distortion in microwave phase shifters based on slow and fast light propagation in semiconductor optical amplifiers," *Opt. Lett.*, vol. 35, no. 16, pp. 2762–2764, 2010.

[31] Y. Dong *et al.*, "Photonic microwave phase shifter/modulator based on a nonlinear optical loop mirror incorporating a Mach-Zehnder interferometer," *Opt. Lett.*, vol. 32, no. 7, pp. 745–747, 2007.

[32] M. Pu *et al.*, "Tunable microwave phase shifter based on silicon-on-insulator microring resonator," *IEEE Photon. Technol. Lett.*, vol. 22, no. 12, pp. 869–871, Jun. 15, 2010.

[33] Q. Chang, Q. Li, Z. Zhang, M. Qiu, T. Ye, and Y. Su, "A tunable broadband photonic RF phase shifter based on a silicon microring resonator," *IEEE Photon. Technol. Lett.*, vol. 21, no. 1, pp. 60–62, Jan. 1, 2009.

[34] M. Pu *et al.*, "Widely tunable microwave phase shifter based on silicon-on-insulator dual-microring resonator," *Opt. Exp.*, vol. 18, no. 6, pp. 6172–6182, 2010.

[35] H. Chen, Y. Dong, H. He, W. Hu, and L. Li, "Photonic radio-frequency phase shifter based on polarization interference," *Opt. Lett.*, vol. 34, no. 15, pp. 2375–2377, 2009.

[36] H. Jiang, L. Yan, J. Ye, W. Pan, B. Luo, and X. Zou, "Photonic generation of phase-coded microwave signals with tunable carrier frequency," *Opt. Lett.*, vol. 38, no. 8, pp. 1361–1363, 2013.

[37] Z. Li, W. Li, H. Chi, X. Zhang, and J. Yao, "Photonic generation of phase-coded microwave signal with large frequency tunability," *IEEE Photon. Technol. Lett.*, vol. 23, no. 11, pp. 712–714, Jun. 1, 2011.

[38] K. Wei and A. S. Daryoush, "Self-Forced opto-electronic oscillators using Sagnac-loop PM-IM convertor," *J. Lightw. Technol.*, vol. 38, no. 19, pp. 5278–5285, 2020.

[39] W. Li, W. Sun, W. Wang, L. Wang, J. Liu, and N. Zhu, "Photonic-assisted microwave phase shifter using a DMZM and an optical bandpass filter," *Opt. Exp.*, vol. 22, no. 5, pp. 5522–5527, 2014.

[40] J. Shen, G. Wu, W. Zou, and J. Chen, "A photonic RF phase shifter based on a dual-parallel Mach–Zehnder modulator and an optical filter," *Appl. Phys. Exp.*, vol. 5, no. 7, pp. 072502, 2012.

[41] Z. Li *et al.*, "Linear photonic radio frequency phase shifter using a differential-group-delay element and an optical phase modulator," *Opt. Lett.,* vol. 35, no. 11, pp. 1881–1883, 2010.

[42] W. Li, W. Zhang, and J. Yao, "A wideband 360° photonic-assisted microwave phase shifter using a polarization modulator and a polarization-maintaining fiber Bragg grating," *Opt. Exp.*, vol. 20, no. 28, pp. 29838–29843, 2012.

[43] W. Zhang and J. Yao, "Ultrawideband RF photonic phase shifter using two cascaded polarization modulators," *IEEE Photon. Technol. Lett.*, vol. 26, no. 9, pp. 911–914, 1 May 1, 2014.

[44] Y. Zhang and S. Pan, "Broadband microwave signal processing enabled by polarization-based photonic microwave phase shifters," *IEEE J. Quantum Electron.*, vol. 54, no. 4, Aug. 2018, Art. no. 0700112.

[45] S. Pan and Y. Zhang, "Tunable and wideband microwave photonic phase shifter based on a single-sideband polarization modulator and a polarizer," *Opt. Lett.*, vol. 37, no. 21, pp. 4483–4485, 2012.

[46] Y. Zhang, F. Zhang, and S. Pan, "Optical single sideband polarization modulation for radio-over-fiber system and microwave photonic signal processing," *Photon. Res.*, vol. 2, no. 4, Aug. 2014, Art. no. B80.

[47] Y. Zhang, H. Wu, D. Zhu, and S. L. Pan, "An optically controlled phased array antenna based on single sideband polarization modulation," *Opt. Exp.*, vol. 22, no. 4, pp. 3761–37654, 2014.

[48] D. Dolfi, F. Michel-Gabriel, S. Bann, and J. Huignard, "Two-dimensional optical architecture for time-delay beam forming in a phased-array antenna," *Opt. Lett.*, vol. 16, no. 4, pp. 255–257, 1991.

[49] A. Goutzoulis, D. Davies, and J. Zomp, "Hybrid electronic fiber optic wavelength-multiplexed system for true time delay steering of phased array antennas," *Opt. Eng.*, vol. 31, no. 11, pp. 2312–2322, 2005.

[50] S. Kemmet, M. Mina, and R. Weber, "Magnetic pulse generation for high-speed magneto-optic switching," *J. Appl. Phys.*, vol. 109, no. 7, 2011, Art. no. 07E333.

[51] B. Howley, X. Wang, M. Chen, and R. Chen, "Reconfigurable delay time polymer planar lightwave circuit for an X-band phased-array antenna demonstration," *J. Lightw. Technol.*, vol. 25, no. 3, pp. 883–890, 2007.

[52] J. Shin, B. Lee, and B. Kim, "Optical true time-delay feeder for X-band phased array antennas composed of 2×2 optical MEMS switches and fiber delay lines," *IEEE Photon. Technol. Lett.*, vol. 16, no. 5, pp. 1364–1366, May 2004.

[53] G. Hu *et al.*, "Optical beamformer based on diffraction order multiplexing (DOM) of an arrayed waveguide grating," *J. Lightw. Technol.*, vol. 37, no. 13, pp. 2898–2904, 2019.

[54] Z. Cao, X. Zhao, F. M. Soares, N. Tessema, and A. M. J. Koonen, "38-GHz millimeter wave beam steered fiber wireless systems for 5G indoor coverage: Architectures, devices, and links," *IEEE J. Quantum Electron.*, vol. 53, no. 1, Feb. 2017, Art. no. 8000109.

[55] O. Raz, S. Barzilay, R. Rotman, and M. Tur, "Submicrosecond scan-angle switching photonic beamformer with flat RF response in the c and x bands," *J. Lightw. Technol.*, vol. 26, no. 15, pp. 2774–2781, 2008.

[56] A. Yu, W. Zou, S. Li, and J. Chen, "A multi-channel multi-bit programmable photonic beamformer based on cascaded DWDM," *IEEE Photon. J.*, vol. 6, no. 4, pp. 1–10, Aug. 2014.

[57] A. Molony, C. Edge, and I. Bennion, "Fibre grating time delay element for phased array antennas," *Electron. Lett.*, vol. 31, no. 17, pp. 1485–1486, 1995.

[58] J. Corral, J. Marti, J. Fuster, and R. Laming, "True time-delay scheme for feeding optically controlled phased-array antennas using chirped-fiber gratings," *IEEE Photon. Technol. Lett.*, vol. 9, no. 11, pp. 1529–1531, Nov. 1997.

[59] N. Srivastava, R. Parihar, and S. Raghuwanshi, "Efficient photonic beamforming system incorporating a unique featured tunable chirped fiber bragg grating for application extended to the Ku-band," *IEEE Trans. Microw. Theory Techn.*, vol. 68, no. 5, pp. 1851–1857, May 2020.

[60] M. Y. Chen, H. Subbaraman, and R. T. Chen, "Photonic crystal fiber beamformer for multiple X-band phased-array antenna transmissions," *IEEE Photon. Technol. Lett.*, vol. 20, no. 5, pp. 375–377, Mar. 1, 2008.

[61] S. García, R. Guillem, and I. Gasulla, "Ring-core few-mode fiber for tunable true time delay line operation," *Opt. Exp.*, vol. 27, no. 22, pp. 31773–31782, 2019.

[62] X. Zou, W. Pan, B. Luo, and L. Yan, "Wavelength demodulation approach based on dispersion-induced microwave power fading for optical sensor," *IEEE Sensors J.*, vol. 12, no. 5, pp. 1267–1271, May 2012.

[63] G. Smith, D. Novak, and Z. Ahmed, "Technique for optical SSB generation to overcome dispersion penalties in fibre-radio systems," *Electron. Lett.*, vol. 33, no. 1, pp. 74–75, 1997.

[64] J. Corral, J. Marti, J. Fuster, and R. Laming, "Dispersion-induced bandwidth limitation of variable true time delay lines based on linearly chirped fibre gratings," *Electron. Lett.*, vol. 34, no. 2, pp. 209–211, 1998.

[65] X. Xue, X. Zheng, H. Zhang, and B. Zhou, "Mitigation of RF power degradation in dispersion-based photonic true time delay systems," in *Proc. IEEE Top. Meet. Microw. Photon.*, 2010, pp. 93–95.

[66] P. Maak, I. Frigyes, L. Jakab, I. Habermayer, M. Gyukics, and P. Richter, "Realization of true-time delay lines based on acoustooptics," *J. Lightw. Technol.*, vol. 20, no. 4, pp. 730–739, 2002.

[67] X. Yi, L. Li, T. Huang, and R. Minasian, "Programmable multiple true-time-delay elements based on a fourier-domain optical processor," *Opt. Lett.*, vol. 37, no. 4, pp. 608–610, 2012.

[68] A. Zadok, O. Raz, A. Eyal, and M. Tur, "Optically controlled low-distortion delay of GHz-wide radio-frequency signals using slow light in fibers," *IEEE Photon. Technol. Lett.*, vol. 19, no. 7, pp. 462–464, Apr. 1, 2007.

[69] P. Berger, J. Bourderionnet, F. Bretenaker, D. Dolf, and M. Alouini, "Time delay generation at high frequency using soa based slow and fast light," *Opt. Exp.*, vol. 19, no. 22, pp. 21180–21188, 2011.

[70] X. Ye, F. Zhang, and S. Pan, "Compact optical true time delay beamformer for a 2D phased array antenna using tunable dispersive elements," *Opt. Lett.*, vol. 41, no. 17, pp. 3956–3959, 2016.

[71] X. Ye, F. Zhang, and S. Pan, "Optical true time delay unit for multi-beamforming," *Opt. Exp.*, vol. 23, no. 8, pp. 10002–10008, 2015.

[72] J. Yao and Q. Wang, "Photonic microwave bandpass filter with negative coefficients using a polarization modulator," *IEEE Photon. Technol. Lett.*, vol. 19, no. 9, pp. 644–646, May 1, 2007.

[73] H. Zhang, S. Pan, M. Huang, and X. Chen, "Polarization-modulated analog photonic link with compensation of the dispersion-induced power fading," *Opt. Lett.*, vol. 37, no. 5, pp. 866–868, 2012.

[74] F. Zhang *et al.*, "Photonics-based broadband radar for high-resolution and real-time inverse synthetic aperture imaging," *Opt. Exp.*, vol. 25, no. 14, pp. 16274–16281, 2017.

[75] C. Özdemir, "Inverse synthetic aperture radar imaging and its basic concepts," in *Inverse Synthetic Aperture Radar Imaging With MATLAB*. Hoboken, NJ, USA: Wiley, 2012, pp. 121–186.

[76] C. Porzi *et al.*, "Photonic integrated microwave phase shifter up to the mm-wave band with fast response time in silicon-on-insulator technology," *J. Lightw. Technol.*, vol. 36, no. 19, pp. 4494–4500, 2018.

[77] R. Moreira *et al.*, "Integrated ultra-low-loss 4-bit tunable delay for broadband phased array antenna applications," *IEEE Photon. Technol. Lett.*, vol. 25, no. 12, pp. 1165–1168, Jun. 15, 2013.

[78] P. Zheng *et al.*, "A seven bit silicon optical true time delay line for Ka-band phased array antenna," *IEEE Photon. J.*, vol. 11, no. 4, pp. 1–9, Aug. 2019.

[79] S. Abe, M. Chu, T. Sasaki, and K. Hane, "Time response of a micro-electromechanical silicon photonic waveguide coupler switch," *IEEE Photon. Technol. Lett.*, vol. 26, no. 15, pp. 1553–1556, Aug. 1, 2014.

[80] J. Briere *et al.*, "Rotating circular micro-platform with integrated waveguides and latching arm for reconfigurable integrated optics," *Micromachines*, vol. 8, no. 12, pp. 354, Dec. 2017.

[81] P. Dong *et al.*, "Submilliwatt, ultrafast and broadband electro-optic silicon switches," *Opt. Exp.*, vol. 18, no. 24, pp. 25225–25231, 2010.

[82] N. Dupuis *et al.*, "Design and fabrication of low-insertion-loss and low-crosstalk broadband 2 × 2 Mach–Zehnder silicon photonic switches," *J. Lightw. Technol.*, vol. 33, no. 17, pp. 3597–3606, 2015.

[83] A. Yeniay and R. Gao, "True time delay photonic circuit based on perfluorpolymer waveguides," *IEEE Photon. Technol. Lett.*, vol. 22, no. 21, pp. 1565–1567, Nov. 1, 2010.

[84] K. Acoleyen, W. Bogaerts, and R. Baets, "Two-dimensional dispersive off-chip beam scanner fabricated on silicon-on-insulator," *IEEE Photon. Technol. Lett.*, vol. 23, no. 17, pp. 1270–1272, Sep. 1, 2011.

[85] X. Zhang, M. Zhao, Y. Jiao, Z. Cao, and A. Koonen, "Integrated wavelength-tuned optical mm-wave beamformer with doubled delay resolution," *J. Lightw. Technol.*, vol. 38, no. 8, pp. 2353–2359, 2020.

[86] J. Cardenas *et al.*, "Wide-bandwidth continuously tunable optical delay line using silicon microring resonators," *Opt. Exp.*, vol. 18, no. 25, pp. 26525–26534, 2010.

[87] A. Meijerink *et al.*, "Novel ring resonator-based integrated photonic beamformer for broadband phased array receive antennas—Part I: Design and performance analysis," *J. Lightw. Technol.*, vol. 28, no. 1, pp. 3–18, 2010.

[88] Y. Liu, A. Wichman, B. Isaac, J. Kalkavage, and J. Klamkin, "Ring resonator based integrated optical beam forming network with true time delay for mmW communications," in *Proc. IEEE MTT-S Int. Microw. Symp.*, pp. 443–446, 2017.

[89] M. Burla, M. Khan, L. Zhuang, and C. Roeloffzen, "Multiwavelength optical beam forming network with ring resonator-based binary-tree architecture for broadband phased array antenna systems," in *Proc. 13th Annu. Symp. IEEE/LEOS Benelux Chapter*, Enschede, The Netherlands, 2008, pp. 99–102.

[90] J. Poon, L. Zhu, G. DeRose, and A. Yariv, "Transmission and group delay of microring coupled-resonator optical waveguides," *Opt. Lett.*, vol. 31, no. 4, pp. 456–458, 2006.

[91] M. Huang, S. Li, M. Xue, L. Zhao, and S. Pan, "Flat-top optical resonance in a single-ring resonator based on manipulation of fast-and slow-light effects," *Opt. Exp.*, vol. 26, no. 18, pp. 23215–23220, 2018.

[92] S. Pan, Z. Tang, M. Huang, and S. Li, "Reflective-type microring resonator for on-chip reconfigurable microwave photonic systems," *IEEE J. Sel. Topics Quantum Electron.*, vol. 26, no. 5, Sep.-Oct. 2020, Art. no. 7701712.

[93] A. Choudhary *et al.*, "Tailoring of the Brillouin gain for on-chip widely tunable and reconfigurable broadband microwave photonic filters," *Opt. Lett.*, vol. 41, no. 3, pp. 436–439, Feb. 2016.

[94] I. Aryanfar *et al.*, "Chip-based brillouin radio frequency photonic phase shifter and wideband time delay," *Opt. Lett.*, vol. 42, no. 7, pp. 1313–1316, 2017.

[95] N. Tessema, Z. Cao, J. Zantvoort, E. Tangdiongga, A. Smolders, and A. Koonen, "Wavelength-tunable true time delay for multi-beam radio beamformer in multi-Gbps satellite communication," in *Proc. 42nd Eur. Conf. Opt. Commun.*, 2016, pp. 1–3.

[96] A. Melloni, F. Morichetti, C. Ferrari, and M. Martinelli, "Continuously tunable 1 byte delay in coupled-resonator optical waveguides," *Opt. Lett.*, vol. 33, no. 20, pp. 2389–2391, 2008.

[97] F. Morichetti, A. Melloni, A. Breda, A. Canciamilla, C. Ferrari, and M. Martinelli, "A reconfigurable architecture for continuously variable optical slow-wave delay lines," *Opt. Exp.*, vol. 15, no. 25, pp. 17273–17282, 2007.

[98] D. Lin *et al.*, "A tunable optical delay line based on cascaded silicon nitride microrings for Ka-band beamforming," *IEEE Photon. J.*, vol. 11, no. 5, pp. 1–10, 2019.

[99] P. Morton, J. Khurgin, Z. Mizrahi, and S. Morton, "Commercially packaged optical true-time-delay devices with record delays of wide bandwidth signals," in *Proc. Conf. Lasers Electro-Optics - Laser Sci. Photon. Appl.*, 2014, pp. 1–2.

[100] C. Xiang, M. Davenport, J. Khurgin, P. Morton, and J. Bowers, "Low-Loss continuously tunable optical true time delay based on Si_3N_4 ring resonators," *IEEE J. Sel. Topics Quantum Electron.*, vol. 24, no. 4, pp. 1–9, Jul.-Aug. 2018.

[101] L. Zhuang *et al.*, "Novel ring resonator-based integrated photonic beamformer for broadband phased array receive antennas—Part II: Experimental prototype," *J. Lightw. Technol.*, vol. 28, no. 1, pp. 19–31, 2010.

[102] M. Burla *et al.*, "Integrated photonic Ku-band beamformer chip with continuous amplitude and delay control," *IEEE Photon. Technol. Lett.*, vol. 25, no. 12, pp. 1145–1148, Jun. 15, 2013.

[103] Y. Liu *et al.*, "Tuning optimization of ring resonator delays for integrated optical beam forming networks," *J. Lightw. Technol.*, vol. 35, no. 22, pp. 4954–4960, 2017.

[104] Y. Liu *et al.*, "Ultra-low-loss silicon nitride optical beamforming network for wideband wireless applications," *IEEE J. Sel. Topics Quantum Electron.,* vol. 24, no. 4, pp. 1–10, Jul. -Aug. 2018.

[105] N. Tessema *et al.*, "A tunable Si_3N_4 integrated true time delay circuit for optically-controlled K-band radio beamformer in satellite communication," *J. Lightw. Technol.*, vol. 34, no. 20, pp. 4736–4743, 2016.

[106] L. Zhuang, C. Roeloffzen, R. Heideman, A. Borreman, A. Meijerink, and W. Etten, "Single-chip ring resonator-based 1×8 optical beam forming network in CMOS-compatible waveguide technology," *IEEE Photon. Technol. Lett.*, vol. 19, no. 15, pp. 1130–1132, 2007.

[107] G. Choo, C. Madsen, S. Palermo, and K. Entesari, "Automatic monitor-based tuning of RF silicon photonic true-time-delay beamforming networks," in *Proc. IEEE/MTT-S Int. Microw. Symp.*, 2018, pp. 1192–1194.

[108] F. Xia, L. Sekaric, and Y. Vlasov, "Ultracompact optical buffers on a silicon chip," *Nature Photon.,* vol. 1, no. 1, pp. 65–71, 2007.

[109] J. Xie, L. Zhou, Z. Li, J. Wang, and J. Chen, "Seven-bit reconfigurable optical true time delay line based on silicon integration," *Opt. Exp.*, vol. 22, no. 19, pp. 22707–22715, 2014.

[110] X. Wang *et al.*, "Continuously tunable ultra-thin silicon waveguide optical delay line," *Optica*, vol. 4, no. 5, pp. 507–515, 2017.

[111] C. Zhu *et al.*, "Silicon integrated microwave photonic beamformer," *Optica*, vol. 7, no. 9, pp. 1162–1170, 2020.

[112] J. Zhou *et al.*, "Electro-optically switchable optical true delay lines of meter-scale lengths fabricated on lithium niobate on insulator using photolithography assisted chemo-mechanical etching," *Chin. Phys. Lett.*, vol. 37, no. 8, 2020, Art. no. 084201.

[113] C. Lin, H. Subbaraman, A. Hosseini, A. Wang, L. Zhu, and R. Chen, "Silicon nanomembrane based photonic crystal waveguide array for wavelength-tunable true-time-delay lines," *Appl. Phys. Lett.*, vol. 101, no. 5, 2012, Art. no. 051101.

[114] F. Zhang, J. Dong, Y. Zhu, X. Gao, and X. Zhang, "Integrated optical true time delay network based on grating-assisted contradirectional couplers for phased array antennas," *IEEE J. Sel. Topics Quantum Electron.*, vol. 26, no. 5, pp. 1–7, Sep. Oct. 2020.

[115] A. Trinidad, Z. Cao, J. Zantvoort, E. Tangdiongga, and A. Koonen, "Broadband and continuous beamformer based on switched delay lines cascaded by optical ring resonator," in *Proc. Opt. Fiber Commun. Conf. Expo.*, San Diego, CA, 2019, pp. 1–3.

[116] J. Bauters *et al.*, "Planar waveguides with less than 0.1 dB/m propagation loss fabricated with wafer bonding," *Opt. Exp.*, vol. 19, no. 24, pp. 24090–24101, 2011.

[117] H. Lee, T. Chen, J. Li, O. Painter, and K. Vahala, "Ultra-low-loss optical delay line on a silicon chip," *Nature Commun.*, vol. 3, no. 1, pp. 1–7, 2012.
[118] G. Li *et al.*, "Ultralow-loss, high-density SOI optical waveguide routing for macrochip interconnects," *Opt. Exp.*, vol. 20, no. 11, pp. 12035–12039, 2012.
[119] J. B. Khurgin, "Dispersion and loss limitations on the performance of optical delay lines based on coupled resonant structures," *Opt. Lett.*, vol. 32, no. 2, pp. 133–135, 2007.
[120] N. Hosseini *et al.*, "Stress-optic modulator in TriPleX platform using a piezoelectric lead zirconate titanate (PZT) thin film," *Opt. Exp.*, vol. 23, no. 11, pp. 14018–14026, 2015.

SHILONG PAN (Senior Member, IEEE) received the B.S. and Ph.D. degrees in electronic engineering from Tsinghua University, Beijing, China, in 2004 and 2008, respectively.

From 2008 to 2010, he was a 'Vision 2010' Postdoctoral Research Fellow with the Microwave Photonics Research Laboratory, University of Ottawa, Canada. He joined the College of Electronic and Information Engineering, Nanjing University of Aeronautics and Astronautics, China, in 2010, where he is currently a Full Professor and an Executive Director of the Key Laboratory of Radar Imaging and Microwave Photonics, Ministry of Education. He has authored or coauthored more than 400 research papers, including more than 200 articles in peer-reviewed journals and 200 papers in conference proceedings. His research interests include microwave photonics, which includes optical generation and processing of microwave signals, analog photonic links, photonics microwave measurement, and integrated microwave photonics.

Prof. Pan is currently an Associate Editor of *Electronics Letters*, a Topical Editor of *Chinese Optics Letters*, and is a Technical Committee member of IEEE MTT-22 Microwave Photonics. He was a Chair of a number of international conferences, symposia, and workshops, including the TPC Chair of the International Conference on Optical Communications and Networks in 2015, and TPC Co-Chair of the IEEE International Topical Meeting on Microwave Photonics in 2017. He is a Fellow of OSA, SPIE, and IET. He was selected as an IEEE Photonics Society Distinguished Lecturer in 2019 and 2020.

XINGWEI YE (Student Member, IEEE) received the B.S. degree in 2014 from the Nanjing University of Aeronautics and Astronautics, Nanjing, China, where he is currently working toward the Ph.D. degree with the Key Laboratory of Radar Imaging and Microwave Photonics, Ministry of Education.

His main research interests include photonic technologies for RF beamforming, synthetic aperture imaging, and direct sampling.

YAMEI ZHANG (Member, IEEE) received the B.S. and Ph.D. degrees from Nanjing University of Aeronautics and Astronautics, Nanjing, China, in 2012 and 2018, respectively.

She is currently with the Key Laboratory of Radar Imaging and Microwave Photonics and the Ministry of Education, Nanjing University of Aeronautics and Astronautics, Nanjing, China. Her research interests include microwave photonic signal generation and processing, and ultra-fast microwave photonics.

FANGZHENG ZHANG (Senior Member, IEEE) received the B.S. degree from Huazhong University of Science and Technology, Wuhan, China, in 2008, and the Ph.D. degree from Beijing University of Posts and Telecommunications, Beijing, China, in 2013.

He is currently a Professor with the Key Laboratory of Radar Imaging and Microwave Photonics and the Ministry of Education, Nanjing University of Aeronautics and Astronautics, Nanjing, China. His current research interest includes microwave photonics, radar imaging, and machine learning.